

Article

Structural Characterization of Fine γ' -Fe₄N Nitrides Formed by Active Screen Plasma Nitriding

Jaroslav Jan Jasinski ^{1,*}, Lukasz Kurpaska ², Tadeusz Fraczek ³, Malgorzata Lubas ³ and Maciej Sitarz ⁴

¹ Department of Innovation and Safety Systems, Czestochowa University of Technology CUT, 42-200 Czestochowa, Poland

² Materials Research Laboratory, National Center for Nuclear Research, 05-500 Swierk–Otwock, Poland; lukasz.kurpaska@ncbj.gov.pl

³ Department of Materials Engineering, Czestochowa University of Technology CUT, 42-200 Czestochowa, Poland; tadeusz.fraczek@pcz.pl (T.F.); malgorzata.lubas@pcz.pl (M.L.)

⁴ Faculty of Materials Science and Ceramics, AGH University of Science and Technology, 30-059 Cracow, Poland; msitarz@agh.edu.pl

* Correspondence: jaroslav.jasinski@pcz.pl; Tel.: +48-507941657

Received: 9 November 2020; Accepted: 7 December 2020; Published: 9 December 2020



Abstract: The paper presents the structural characterization of γ' -Fe₄N nitrides produced by active screen plasma nitriding (ASPN) processes. Experiments were performed on the Fe-Armco model material at 693, 773, and 853 K for 6 h. Investigation of the properties of the substrate was realized using scanning electron microscopy (SEM, SEM–EBSD/Kikuchi lines), energy-filtered transmission electron microscopy (TEM-EFTEM), X-ray diffraction (GID, grazing incidence diffraction, micro-XRD), and secondary ion mass spectroscopy (SIMS). Results have confirmed that the γ' -Fe₄N nitrides' structure and morphology depend considerably on the nitriding process's plasma conditions and cooling rate. In addition to that, γ' -Fe₄N nitrides' formation can be correlated with the surface layer saturation mechanism and recombination effect. It has been shown that the γ' -Fe₄N structure depends considerably on several phenomena that occur in the diffusive layer (e.g., top layer decomposition, nitrogen, and carbon atoms' migration). Our research proves that the nitrogen concentration gradient is a driving force of nitrogen migration atoms during the recombination of γ' -Fe₄N nitrides. Finally, realized processes have allowed us to optimize active screen plasma nitriding to produce a surface layer of fine nitrides.

Keywords: surface layer; active screen plasma nitriding; Fe-armco; γ' -Fe₄N nitrides

1. Introduction

Nitriding in plasma conditions is a group of processes that involve the formation of a diffusion layer on the metallic substrates. During this process, the material is submitted to low-temperature, non-isothermal, and low-pressure plasma. The primary role of plasma in the production of nitride layers is to generate charged electrons, ions, excited atoms, and particles with increased energy levels. During the ion-nitriding process, nitrogen in atomic and ionic form is obtained due to excitation, ionization, and dissociation of the nitrogen/hydrogen or ammonia atmosphere [1]. Nitrogen active species formed in the gaseous plasma changes the reaction at the surface and affects the diffusion zone formation's kinetics by changing the substrate energy and inducing sorption processes. This increases the number of new reactions at the plasma/substrate interface and highly improves the layer's adhesion [2]. Generally, conventional cathode plasma nitriding (CPN) is realized in vacuum reactors at a 400–1000 V; the low vacuum of 300 Pa–1 hPa; pressure ≥ 1 Pa and a temperature range 693–853 K. The composition of the

nitriding atmosphere is fixed during the process and remains the same during the gas's continuous flow through the reactor (dynamic vacuum). Voltage is applied directly to the cathode, which causes the so-called cathodic drop, accompanied by the glow effect [3,4]. In the initial stage of plasma nitriding processes, an important role is played by argon gas, a carrier of high-energy particles used for heating the workpiece (substrate). As a result of interaction with particles in the plasma, argon also promotes an increase in electron density and affects energy transfer during collisions. Likewise, due to the surface bombardment with argon ions, the substrate surface is simultaneously cleaned and activated. Surface activation increases the density of dislocations, Frenkel defects, and diffusion paths, affecting further nucleation of nitride phases in the plasma nitriding process [5,6]. However, by the fact that the conventional cathode plasma nitriding (CPN) method has some disadvantages associated with, for instance, too intensive spraying of the workpiece edges (edge effect) which may cause their damage, a novel solution to prevent such effects called active screen plasma nitriding (ASPN) was introduced and patented by Georges [7]. In the ASPN process, the substrate is arranged in plasma potential (or connected with the cathode) and covered with a perforated cylindrical element (screen, mesh, cage). The active screen's role lies in the increased intensity of the sample heating up to the nitriding process temperature and effective ion bombardment and the delivery of high-energy nitrogen particles to the substrate surface, finally obtaining a high surface concentration of nitrogen. Such effect results in the formation of NH_x radicals, Fe_xN_y compounds, and diffusion into the nitride layer, and formation of ϵ - Fe_{2-3}N , γ' - Fe_4N nitrides [8,9]. The Fe atoms, which are sprayed from the cathodic surface, react in the plasma glow discharge with N_2 , resulting in the formation of metastable FeN nitride. This layer, under the influence of continuous sputtering, decomposes constantly. Afterward, the atomic nitrogen, from the decomposition of non-stoichiometric nitrides, diffuses into the surface layer, finally creating a diffusion zone. At the same time, Fe from the nitrogen-depleted substrate's surface is re-sputtered into the plasma [10–13]. According to the plasma nitriding mechanism presented by Mittemeijer and Keddani [14,15], the diffusion rate is higher at the $\text{Fe}_\alpha(\text{N,C})/\gamma'$ - Fe_4N interface than at the γ' - $\text{Fe}_4\text{N}/\epsilon + \gamma'$ interface and diffusion of nitrogen through the matrix occurs, rapidly creating the $\text{Fe}_\alpha(\text{N,C}) + \gamma'$ - Fe_4N diffusion zone. However, to investigate γ' - Fe_4N nitrides' formation mechanism in ASPN nitriding, other process conditions need to be considered, such as the distance between the active screen and the workpiece. If the distance between the active screen and the substrate is small, the material sprayed from the screen is dispersed over a small area, thus creating a thin layer which inhibits the formation of nitride layers. Therefore, to ensure the nitriding process is effective, the active screen should be placed at such distance that high-energy particles, migrating from the screen to the substrate, reach the surface properly charged [16–19]. Plasma research has shown that the kinetic energy of the reactive species and their flux has a significant impact on nitrogen concentration, thus on nitrided layer formation and its properties (e.g., hardness, depth, topography). Using the active screen, we can produce more high-energy particles that collide, creating new compounds at the substrate surface [20–22]. The tests carried out on the free path of particles in the active screen nitriding process have shown that N^+ ions accelerate with a potential of ca. 1.25 kV and in ammonia atmosphere with a density of $2.6 \times 10^{-3} \text{ kg}\cdot\text{m}^{-3}$, a free path of even 70 mm can be reached. This suggests that a significant amount of high-energy nitrogen species generated under the active screen can reach the substrate surface. These particles have velocities that are at the limit values of the γ' - Fe_4N phase formation in which energy activation due to the higher mobility of nitrogen ions is smaller in ASPN than in the CPN process and equals $-64.0 \text{ kJ}\cdot\text{mol}^{-1}$ and $-73.2 \text{ kJ}\cdot\text{mol}^{-1}$ respectively [23–25]. Based on the reported values, one can see that the difference is significant and associated with the high non-equilibrium of ionization during the ASPN process. Therefore the research's primary purpose was to investigate the effect of fine Fe_4N nitrides formation, especially for the applied active screen method. The results showed some significant differences between CPN and ASPN in the structure of γ' - Fe_4N nitride.

2. Materials and Methods

Pure iron (Fe-Armco) substrates ($20 \times 20 \times 5 \text{ m}^3$) were mechanically activated with metallographic paper (up to 2000 grit). In the next stage, samples were cleaned with ethanol and placed into the plasma nitriding reactor. Two variants of the nitriding process were realized: I. CPN; and II. ASPN. Processes were carried out using the cooled anode reactor shown in Figure 1.

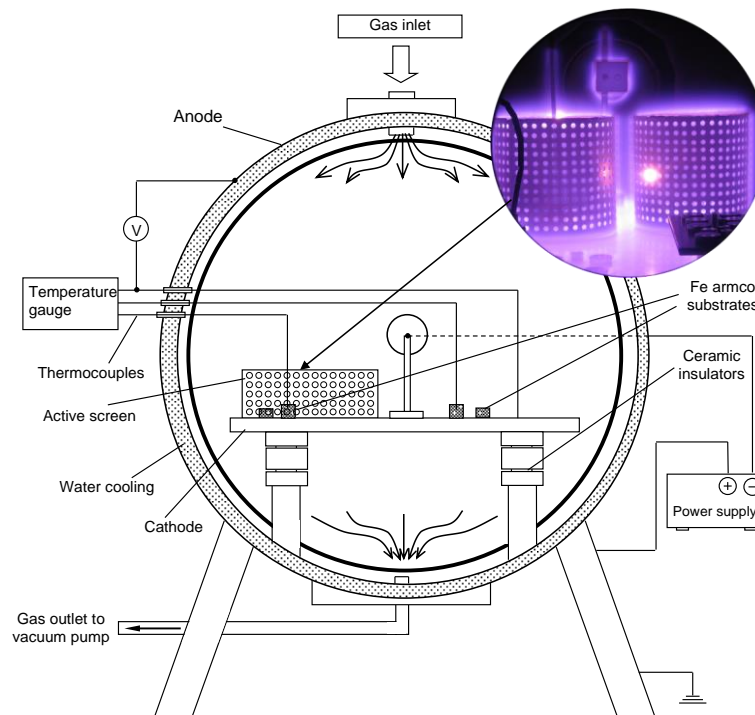


Figure 1. Schematic view of a plasma nitriding reactor along with Fe-Armco substrates placement on the cathode and under the active screen.

The cathode of the reactor and active screen material was AISI 1010 low-carbon steel so that there is no influence of alloying elements on the substrate surface. During the ASPN nitriding, the distance between the substrate and the active screen was 90 mm. Surface ion activation (sputtering) was performed during the workpiece's heating up to the nitriding temperature. Detailed parameters of the plasma nitriding processes are presented in Table 1.

Table 1. Parameters of the cathode plasma nitriding (CPN) and active screen plasma nitriding (ASPN) of Fe-Armco substrates.

Parameter	Sputtering	Plasma Nitriding
Atmosphere [%]	90% H ₂ –10% Ar	25% N ₂ –75% H ₂
Temperature [K]	heating up to process	693, 773, 853
Treatment time [h]	~0.8–1	6
Pressure [Pa]	150	150
Voltage [V]	~750	~860
Effective power [kW]	~5.4	~5.2

In order to investigate the structure of the nitrided layer produced with CPN and ASPN processes, a series of studies were conducted. Microscopic observations to verify morphology, structure, and dispersion rate of the layers were conducted by scanning electron microscopy (SEM, JEOL JSM-6610LV microscope, Tokyo Japan). Phase composition analysis was realized using the SEM–EBSD/Kikuchi lines method (HITACHI SU70 microscope with Thermo Scientific (Ibaraki, Japan) analytical equipment)

and the X-ray diffraction methods grazing incidence diffraction (GIXRD) and micro-X-ray diffraction (μ -XRD). Structural characterization of the γ' -Fe₄N compounds and nitrogen concentration maps were realized by the energy-filtered transmission electron microscopy (EFTEM) method (FEI TITAN 80–300 microscope, Waltham, MA, USA). The nitrided layer depth was analyzed by the secondary ion mass spectroscopy (SIMS) method (CAMECA IMS 6F spectrometer, Gennevilliers, France).

3. Results and Discussion

The results of the plasma nitriding processes (CPN and ASPN) allowed us to identify the type of γ' -Fe₄N nitrides morphology and verify the influence of different process conditions on nitrogen transport and its concentration in the nitride layer. Formation of γ' -Fe₄N nitrides in the active screen plasma nitriding is a consequence of the recombination mechanism as a result of the rapid transition from a metastable state to a stable state, where non-stoichiometric nitrides γ' -Fe₄N_{1-x}, in consequence of high-energy nitrogen species saturation, tend to obtain stoichiometry and create fine γ' -Fe₄N phases, whereas in the cathode plasma nitriding variant, the γ' -Fe₄N nitrides are in the form of thick, brittle needles. The active screen effect is here particularly useful due to the reduction in the temperature of the process and changing the driving force of the γ' -Fe₄N nitride phase nucleation during nitriding, especially at a temperature below 793 K. The studies conducted have also shown that the γ' -Fe₄N nitrides formed by the ASPN process have higher activity and can more easily adsorb nitrogen particles from the Fe₂N, ϵ -Fe₂₋₃N + γ' -Fe₄N compounds finally to form desired fine structures [26–28]. Figure 2 shows the Fe-Armco surface's images after cathode plasma nitriding and active screen plasma nitriding processes at 693, 773, and 853 K, respectively. In the nitride layer formed, the following zones and interfaces can be observed: zone I: ϵ -Fe₂₋₃N_{1-x} nitrides (white layer) with nitrogen concentration ranging from 4.55% to 11% (mass volume); zone II: ϵ -Fe₂₋₃N_{1-x} + γ' -Fe₄N_{1-x} layer which is a mixture of ϵ -Fe₂₋₃N_{1-x} and γ' -Fe₄N_{1-x} nitrides and is formed from the decomposition of the white layer; zone III: Fe_α(N,C) which is a solid solution of nitrogen in ferrite; zone IV: γ' -Fe₄N_{1-x} nitrides forming a nitrogen solid solution based on the Fe₄N compound. In zone IV, nitrogen is located in the middle point of the elementary cell with $a_0 = 3.791 \div 3.801 \text{ \AA}$ and consists of precipitates from Fe_α(N,C). These precipitates have often a needle or fine shape and are formed in the plasma process and during the cooling stage from process temperature to room temperature.

Substrates nitrided at 693 K for 6 h with the ASPN method are characterized by a smaller layer thickness than those obtained during the CPN process. Besides, a defected zone which is being created in the process of surface ion sputtering. The results suggest that surface slowly undergoes recrystallization processes related to the slower stress relaxation of the defected surface at the stage preceding nitriding in the presence of the active screen. This phenomenon occurs by the process of linear defects elimination from the structure, i.e., annihilation. In the ASPN process, nitrogen is located in the $\epsilon + \gamma'$ zone and forms an approximately 2 μm compound zone. It is a consequence of ion bombardment and more effective saturation of the surface layer. This zone is being formed in the deformed surface region, suggesting that already at a low temperature of plasma nitriding (693 K), saturation effects and nitrogen concentration are more significant in the ASPN process. The role of the active screen is also enhancing samples heating to the temperature of the nitriding process, as a result of both ion bombardment and thermal radiation from the surface of the heated active screen, as well as to continuously deliver highly energetic excited nitrogen species to the surface of the substrate in order to produce a high concentration of nitrogen at the surface. These effects are associated with increasing the gas phase activity (change of electric field intensity and pressure) due to ionization, which influences nitrogen ions transported to the substrate and changes the equilibrium at the plasma/substrate interface. As the temperature under the active screen rises, at constant pressure, there is an increase in the free path between successive collisions of the plasma components, thus giving them more kinetic energy, which increases the ionization and allows the more ionized gas particles to carry more electric charges from the power source. However in cathode nitriding, there are difficulties resulting from the lack of such highly energetic particles and an identical atmosphere flow on the nitrided substrate's surface,

which finally inhibits the incubation stage of nitride phase formation. In the case of nitriding performed at 773 K for 6 h, the ASPN nitrided layer composed of fine γ' -Fe₄N phase is ca. 38 μm thick, and the compound zone ($\epsilon + \gamma'$) is 3.5 μm . In the nitrided layer obtained by ASPN, few coarse γ' -Fe₄N nitrides formed at the grain boundaries can be spotted (Figure 2), which is a consequence of the recombination of fine γ' -Fe₄N precipitates, which effect will be further discussed and confirmed by the EFTEM results (see Figure 7). Important information on the phenomena and effects during plasma nitriding is given by the results obtained at 853 K. In this case, needle-shaped γ' -Fe₄N nitride layer was visible both after CPN and ASPN process and is approx. 250 μm thick. The porous and flaky white layer (ϵ -Fe₂₋₃N) zone of thickness up to 3 μm was also observed (Figure 2, images for T = 853 K). The pores in the white layer were from 0.5 to 1 μm . At 853 K nitriding process substrates, the surface compound layer's depth after the ASPN and CPN process were 4 and 5.5 μm , respectively. It was also confirmed by SIMS results (Figure 3b,c).

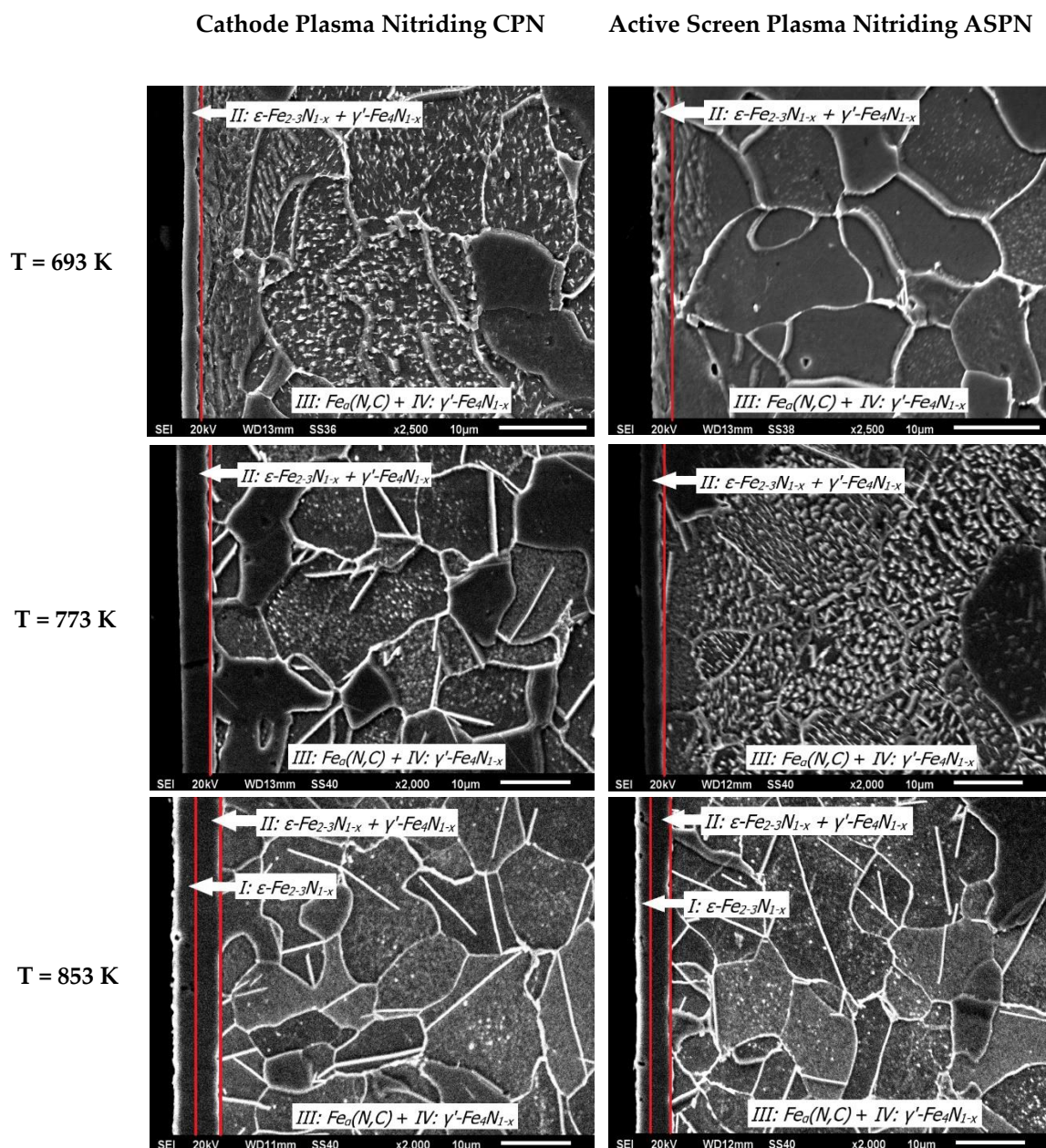


Figure 2. Scanning electron microscopy (SEM) image of the Fe-Armco surface layer obtained after CPN and ASPN processes at 693, 793, 853 K for 6 h in 75% H₂–25% N₂ atmosphere, Nital etched.

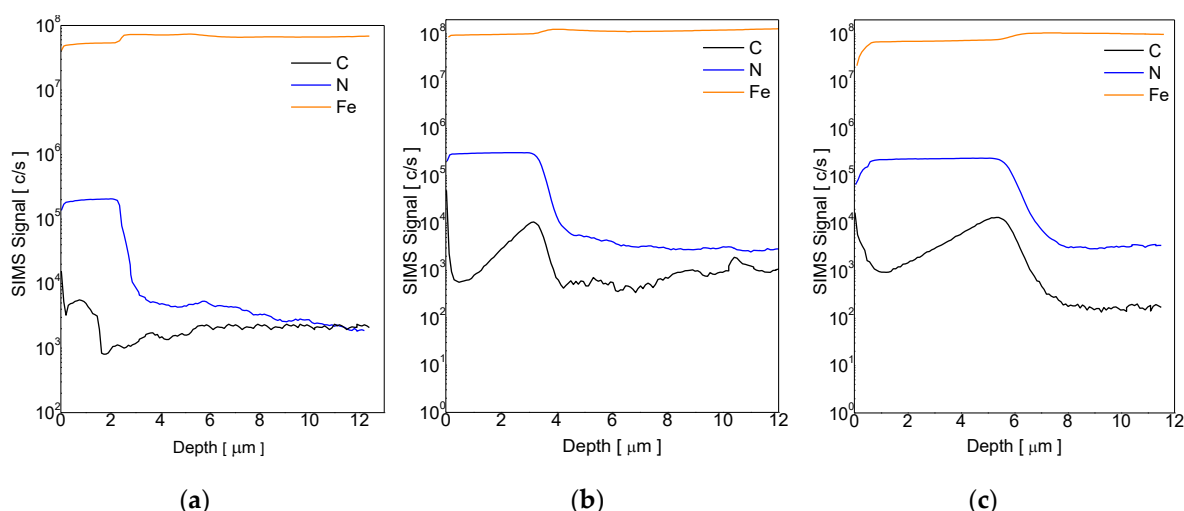


Figure 3. Secondary ion mass spectroscopy (SIMS) profiles of N,C, Fe concentration in the Fe-Armco top layer ($\epsilon+\gamma'$) after active screen plasma nitriding ASPN at (a) 693 K/6 h; (b) 773 K/6 h; (c) 853 K/6 h in 75% H_2 –25% N_2 atmosphere.

The next step of the nitrides phase characterization was X-ray grazing incidence diffraction experiments. Results showed that in the substrates after the ASPN process at 693 K for 6 h, no reflections from the ϵ - Fe_{2-3}N phase (white layer), located around 2θ angle = 44° , can be seen. These reflections are visible in the CPN variant (blue and black peaks in Figure 3a). This phenomenon may result from the solution zone's intensive saturation, limiting ϵ - Fe_{2-3}N phase thickness, or total disappearance at low temperatures due to the complete transition to the γ' - Fe_4N phase. GIXRD patterns recorded at 853 K temperature (Figure 4b) depict this phase regardless of the treatment method. Low-intensity reflections characteristic for the ϵ - Fe_{2-3}N phase in the $2\theta = 44^\circ$ angle can be spotted, see Figure 4b.

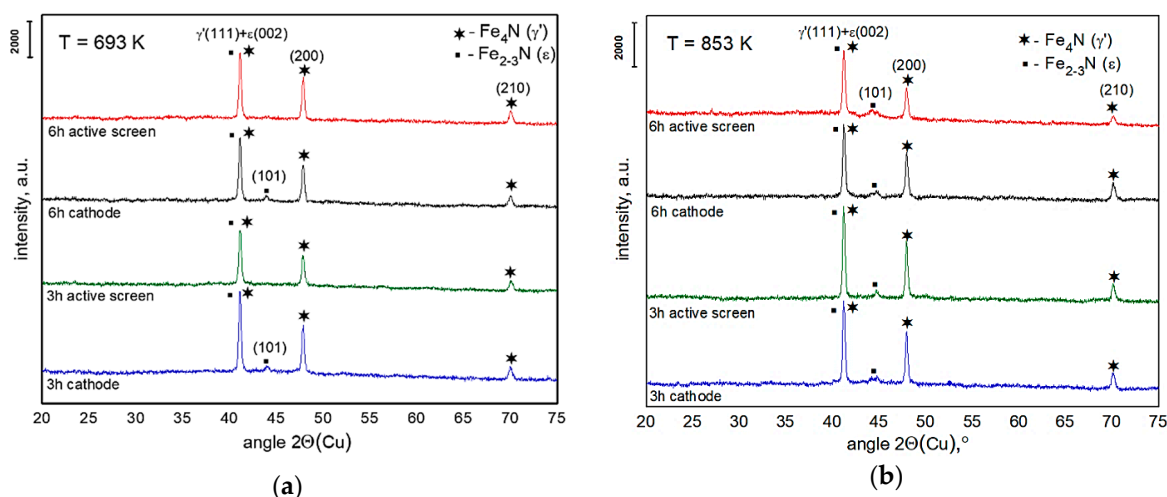


Figure 4. X-ray grazing incidence diffraction patterns of the Fe-Armco after CPN and ASPN process for 3 and 6 h at a temperature of (a) 693 K, (b) 853 K.

GIXRD analysis after both plasma nitriding variants indicated the presence of the ϵ - Fe_{2-3}N + γ' - Fe_4N phase (compound layer) with the crystallographic orientation (111)//(002), which corresponds to the reflex at $2\theta = 41.5^\circ$, and was registered for both phases. The intensive reflex was also noticed from the γ' - Fe_4N nitride phase at an angle of $2\theta = 47.5^\circ$. This reflex corresponds to the crystallographic orientations of (200) and (210). However, the phase composition of the diffusive layer of Fe substrate was investigated with the μ -XRD method. Results obtained show super-net reflections originating

from the γ' -Fe₄N phase, with crystallographic orientations (210), (211), and (220). The intensity of the reflections differs significantly depending on the nitriding method. In ASPN, the most intensive reflections are from the γ' -Fe₄N phase with the crystallographic orientation of (111) and (200) (Figure 5). This zone in the ASPN method consists of fine γ' -Fe₄N nitrides and nitrogen saturated ferrite.

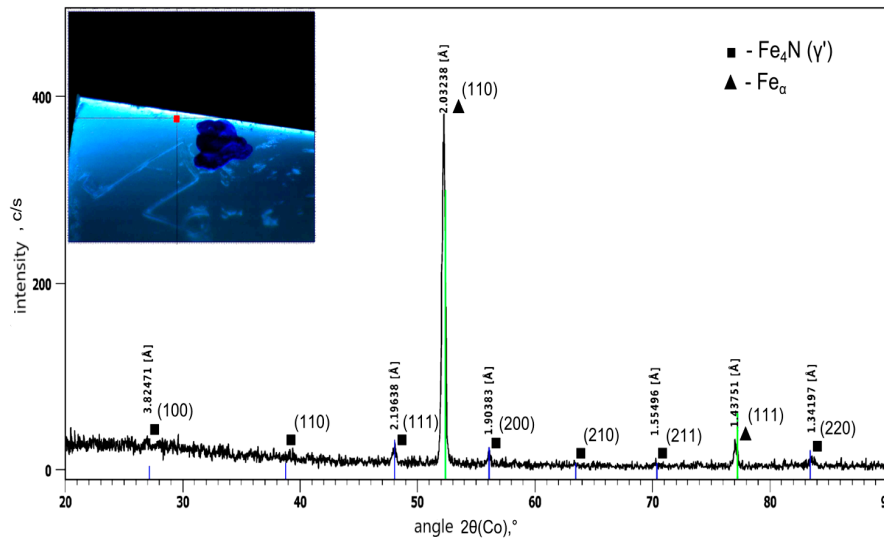


Figure 5. Micro-X-ray diffraction (μ -XRD) diffractogram of Fe Armco after ASPN process at temperature 853 K for 6 h.

γ' -Fe₄N nitride crystallizes in a regular system with a wall-centered cell (fcc), and nitrogen atoms are placed in the spaces between Fe atoms. Simultaneously, the non-stoichiometric phase of ϵ -Fe₂₋₃N has a dense-packed hexagonal crystallographic structure (hcp), and the stoichiometric ϵ phase changes its crystallographic structure to orthorhombic and forms the so-called ζ (Fe₂N) phase. This change is related to the re-arrangement of nitrogen atoms and filling up octahedral gaps and interstitial spaces during the increase in the nitrogen concentration and expansion of the Fe_α elementary cell. Analysis of the EBSD map shows a different orientation of the crystallographic planes at the diffusion zone's surface (γ' -Fe₄N + Fe_α(N,C)). Results suggest that easier nucleation of nitrides in the diffusion zone occurs in the grains with orientation (001). This effect may be related to the change in the diffusion flux velocity for this orientation compared to the (111) orientation. It is expected that it occurs due to the incomplete filling of free areas in octahedral gaps. Consequently, in ASPN, opposite to CPN nitriding, slower delivery of nitrogen atoms (diffusion flux) to grains with orientation (111) leads to faster surface saturation of the substrate. Therefore, a reduction in the formation of brittle coarse needle-shaped γ' -Fe₄N nitrides occurs. Such complex nucleation mechanisms of fine γ' -Fe₄N nitrides and their nucleation in nitrogen ferrite grains are triggered by re-combination phenomena. Additionally, the use of Kikuchi line maps was made to determine the intersected planes' location (hkl) on which the deflection occurred for a given crystalline orientation (Figure 6). Maps have indicated the following phases: γ' -Fe₄N nitride cell in a regular face-centered-cubic (fcc) system, Fe_α(N,C) nitrogen ferrite in a body-centered-cubic (bcc) regular system, and ϵ -Fe₂₋₃N nitride in close-packed hexagonal (hcp) system see Figure 6.

Cathode Plasma Nitriding, T = 773 K, 6 h

Active Screen Plasma Nitriding, T = 773 K, 6 h

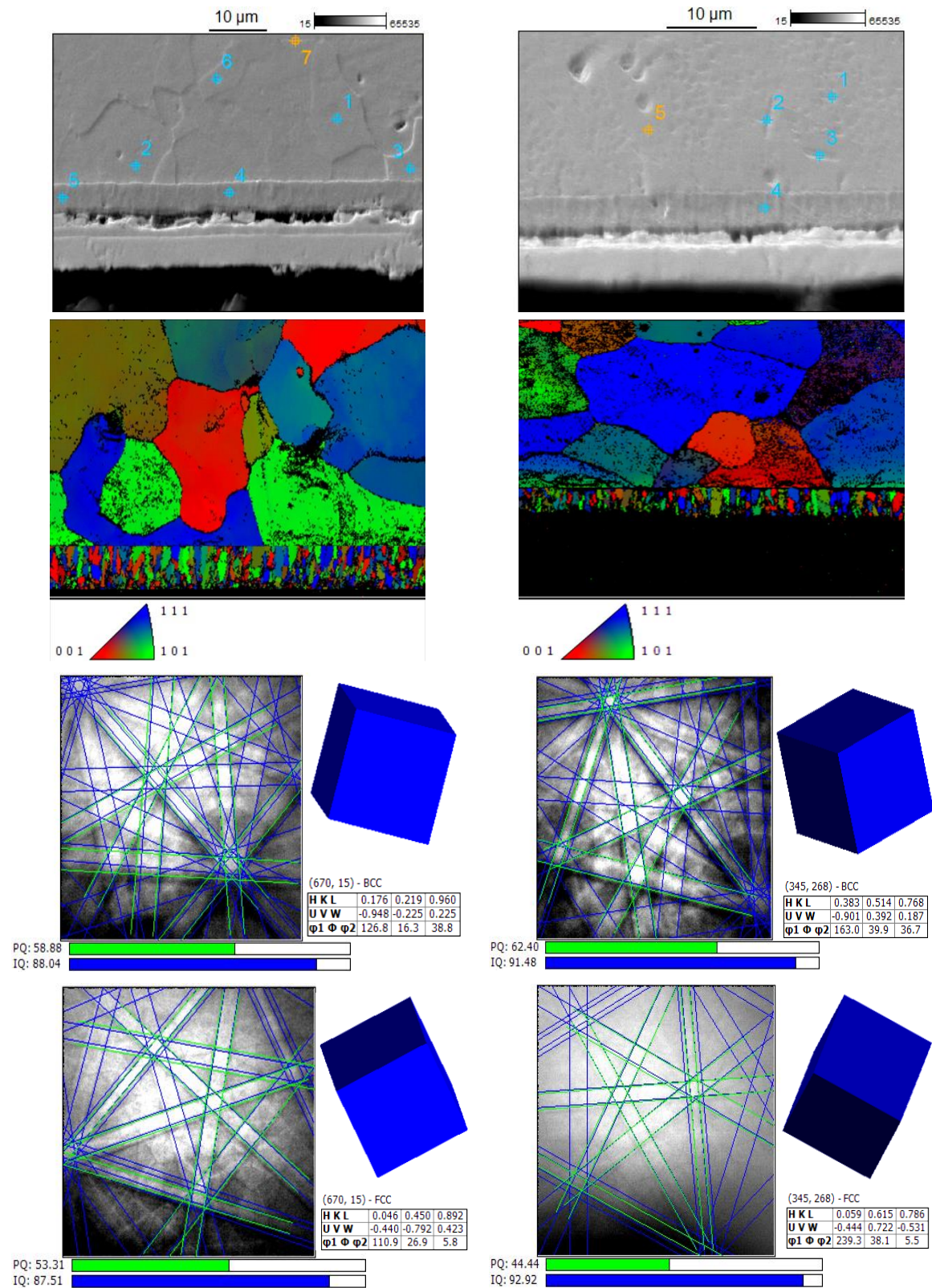


Figure 6. SEM-EBSD maps and Kikuchi lines of the Fe_α(C,N) phase-bcc and γ'-Fe₄N nitrides-fcc phase (EBSD HKL Technology analysis) in the surface layer of Fe-Armco after CPN and ASPN processes at 773 K for 6 h.

The driving force of diffusion in plasma nitriding is a gradient of the chemical potential of atoms diffusing to the matrix of the substrate. Therefore atoms, depending on their physicochemical properties, can diffuse from a higher concentration to a single-phase area. This phenomenon changes the diffusion flux during the diffusion zone formation and γ' -Fe₄N nitrides. It is known that the enthalpy of nitride formation is ca. 11.08 kJ·mol⁻¹ [29]. Therefore, the nucleation of γ' -Fe₄N nitride phases can occur with their complete coherence and mismatch of the network from the matrix through dislocations to the grain boundaries. The fine γ' -Fe₄N zones can be associated with the formation of metastable, non-stoichiometric nitrides γ' -Fe₄N_{1-x}, which in consequence of further nitrogen saturation tend to achieve stoichiometry and as a result of the recombination process transit from a metastable to a more stable state and form fine γ' -Fe₄N structures (Figure 7).

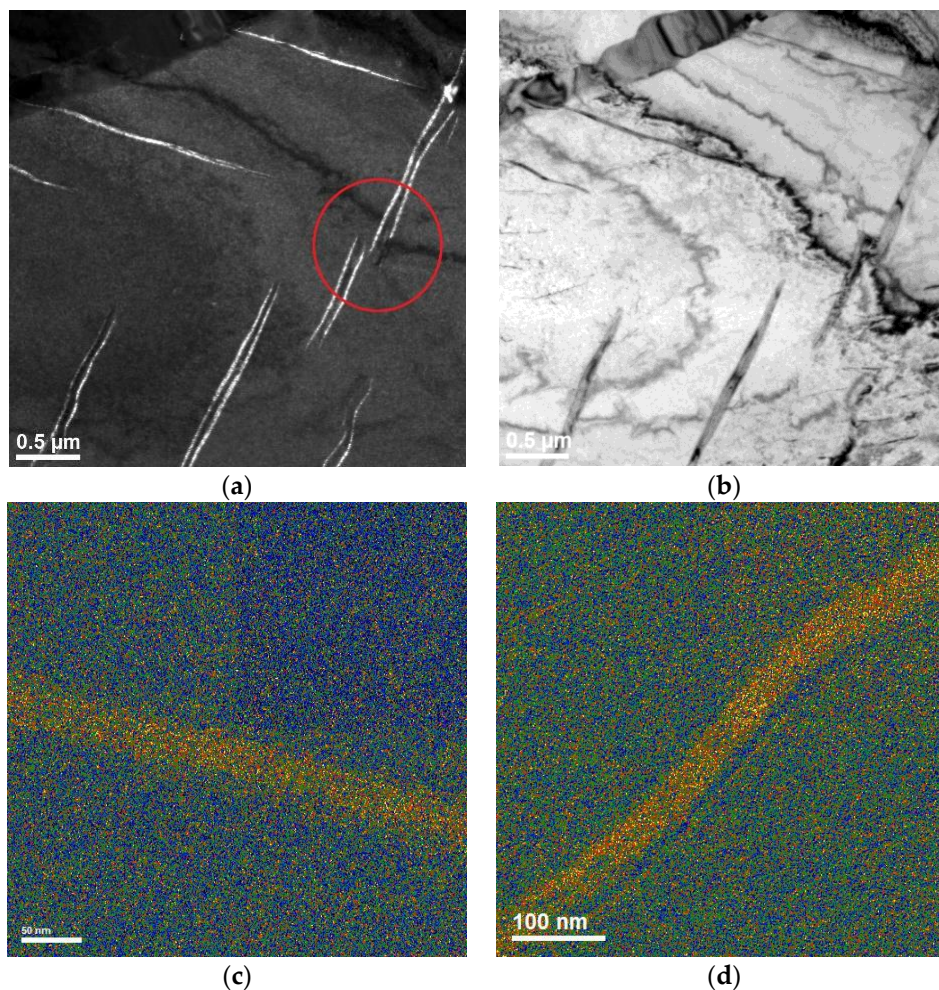


Figure 7. Energy-filtered transmission electron microscopy (EFTEM) image of fine γ' -Fe₄N nitrides after active screen plasma nitriding at 773 K for 6 h—(visible effect of recombination—red marker (a,b), and EFTEM nitrogen concentration maps (c,d).

Therefore, when considering issues related to the kinetics of the nitrided layer growth, not only the phenomena occurring in plasma and process conditions should be taken into account but also the nitride phase formation mechanism, including: *I. Nucleation*, *II. Precipitation*, and *III. Recombination*. One of the hypotheses regarding the absence of coarse brittle needle-shaped γ' -Fe₄N nitrides in the ASPN is the reduced intensity of cooling in active screen presence. It is expected that slow cooling after the process hence the formation of brittle needle-shaped γ' -Fe₄N phase. In the case of active screen plasma nitriding, such effect is of great importance and will be discussed in our further research.

4. Conclusions

This study investigated the effects of plasma nitriding processes on the γ' -Fe₄N nitrides structure and morphology. It has been shown that the γ' -Fe₄N nitrides produced by cathode plasma nitriding have a needle shape, where fine structures characterize nitrides produced in the active screen plasma nitriding. We also investigated the γ' -Fe₄N phase nucleation mechanism by the recombination effect induced by nitrogen diffusion from the compound layer into the substrate matrix. The influence of increased nitrogen concentration induced by active screen application on the plasma/substrate surface interface has also been demonstrated. Such an effect results from the increasing frequency of collisions between hydrogen and nitrogen particles, and the density increase of highly energetic N₂⁺, N⁺ ions, increased amount of N₂^{*} excited species and NH_x radicals. The active screen plasma nitriding method's attractiveness is also associated with the change in morphology of γ' -Fe₄N nitride precipitates in the diffusion zone. It has been proved that the active screen method, opposite to cathode plasma nitriding, results in the creation of diffusive zones without adverse coarse, brittle needle-shaped γ' -Fe₄N nitrides and reduced $\epsilon+\gamma'$ layer. Finally, the conducted research has shown the advantages of the ASPN technique, especially at 773 K process temperature, and has shown the possibility of optimizing the diffusion layer of metallic substrates, important from a technological point of view.

Author Contributions: Conceptualization, J.J.J., M.L. and L.K.; Methodology, J.J.J., T.F. and M.S.; Data analysis and validation, T.F. and M.S.; Performing research and investigation, J.J.J., T.F.; Writing—original draft preparation, J.J.J., M.L. and L.K.; Writing—review and editing, T.F., M.S.; Supervision, J.J.J., T.F. and M.S.; Funding acquisition, J.J.J., T.F., and M.S. All authors have read and agreed to the published version of the manuscript.

Funding: This research received no external funding.

Conflicts of Interest: The authors declare no conflict of interest.

References

1. Mittemeijer, E.J.; Slycke, J.T. Thermodynamic activities of nitrogen and carbon imposed by gaseous nitriding and carburising atmospheres. *Surf. Eng.* **1996**, *3*, 67–71. [[CrossRef](#)]
2. Zhao, C.; Li, C.X.; Dong, H.; Bell, T. Study on the active screen plasma nitriding and its nitriding mechanism. *Surf. Coat. Technol.* **2006**, *201*, 2320–2325. [[CrossRef](#)]
3. Taherkhani, K.; Soltanieh, M. Evaluation of the formation of compound coatings on aluminium by the new method of active screen plasma nitriding. *Mater. Res. Express* **2019**, *6*, 1–10. [[CrossRef](#)]
4. Fraczek, T.; Olejnik, M.; Jasinski, J.J.; Skuza, Z. Short-term low-temperature glow discharge nitriding of 316L austenitic steel. *Metalurgija* **2011**, *50*, 151–154.
5. Walkowicz, J. On the mechanisms of diode plasma nitriding in N₂–H₂ mixtures under DC-pulsed substrate biasing. *Surf. Coat. Technol.* **2003**, *174–175*, 1211–1219. [[CrossRef](#)]
6. Fraczek, T.; Ogorek, M.; Skuza, Z.; Prusak, R. Mechanism of ion nitriding of 316L austenitic steel by active screen method in a hydrogen-nitrogen atmosphere. *Int. J. Adv. Manuf. Technol.* **2020**, *109*, 1357–1368. [[CrossRef](#)]
7. Georges, J. Nitriding Process and Nitriding Furnace Therefor. U.S. Patent 5,989,363, 23 September 1999.
8. Tibbets, G.G. Role of nitrogen atoms in ion-nitriding. *J. Appl. Phys.* **1974**, *45*, 5072–5073. [[CrossRef](#)]
9. Moszynski, D.; Moszynska, I.; Arabczyk, W. Iron nitriding and reduction of iron nitrides in nanocrystalline Fe–N system. *Mater. Lett.* **2012**, *78*, 32–34. [[CrossRef](#)]
10. Bernal, J.L.; Salas, O.; Figueroa, U.; Oseguera, J. Early stages of gamma prim-Fe₄N_{1-x} nucleation and growth in a post-discharge nitriding reactor. *Surf. Coat. Technol.* **2004**, *177–178*, 665–670. [[CrossRef](#)]
11. Wetzel, M.H.; Schwarz, M.R.; Leineweber, A. High-pressure high-temperature study of the pressure induced decomposition of the iron nitride γ' -Fe₄N. *J. Alloys Compd.* **2019**, *801*, 438–448. [[CrossRef](#)]
12. Jasinski, J.J.; Fraczek, T.; Kurpaska, L.; Lubas, M.; Sitarz, M. Effects of different nitriding methods on nitrated layer structure and morphology. *Arch. Metall. Mater.* **2018**, *63*, 337–345.
13. Jacobs, H.; Rechenbach, D.; Zachwieja, U. Structure determination of γ' -Fe₄N and ϵ -Fe₃N. *J. Alloys Compd.* **1995**, *227*, 10–17. [[CrossRef](#)]

14. Leineweber, A.; Gressmann, T.; Mittemeijer, E.J. Simultaneous control of the nitrogen and carbon activities during nitrocarburising of iron. *Surf. Coat. Technol.* **2012**, *206*, 2780–2791. [[CrossRef](#)]
15. Keddam, M. Surface modification of the pure iron by the pulse plasma nitriding: Application of a kinetic model. *Mater. Sci. Eng. A* **2007**, *462*, 169–173. [[CrossRef](#)]
16. Jiang, Z.; Li, X.; Gu, J.; Hu, M.; Zhu, Z. Isothermal decomposition behavior of the high nitrogen concentration γ -Fe[N] prepared from pure iron. *Appl. Surf. Sci.* **2008**, *254*, 7361–7364. [[CrossRef](#)]
17. Nishimoto, A.; Nagatsuka, K.; Narita, R.; Nii, H.; Akamatsu, K. Effect of the distance between screen and sample on active screen plasma nitriding properties. *Surf. Coat. Technol.* **2010**, *205*, 365–368. [[CrossRef](#)]
18. Hubbard, P.; Partridge, J.G.; Doyle, E.D.; McCulloch, G.D.; Taylor, M.B.; Dowe, S.J. Investigation of nitrogen mass transfer within an industrial plasma nitriding system I: The role of surface deposits. *Surf. Coat. Technol.* **2010**, *204*, 1145–1150. [[CrossRef](#)]
19. Hirsch, T.; Clarke, T.G.R.; Rocha, A.d.S. An in-situ study of plasma nitriding. *Surf. Coat. Technol.* **2007**, *201*, 6380–6386. [[CrossRef](#)]
20. Belmonte, T.; Jaoul, C.; Borges, J.N. Modelling nitrogen atom flux in post-discharge nitriding processes. *Surf. Coat. Technol.* **2004**, *188–189*, 201–206. [[CrossRef](#)]
21. Czerwicz, T.; Michel, H.; Bergmann, E. Low-pressure, high-density plasma nitriding: Mechanisms, technology and results. *Surf. Coat. Technol.* **1998**, *108–109*, 182–190. [[CrossRef](#)]
22. Hosseini, S.R.; Ashrafizadeh, F. Accurate measurement and evaluation of the nitrogen depth profile in plasma nitrided iron. *Vacuum* **2009**, *83*, 1174–1178. [[CrossRef](#)]
23. Somers, M.A.J.; Kooi, B.J.; Maldzinski, L.; Mittemeijer, E.J.; Van Der Horst, A.A.; van der Kraan, A.M.; van der Pers, N.M. Thermodynamics and long-range order of interstitials in an h.c.p. lattice Nitrogen in ϵ -Fe₂N_{1-z}. *Acta Mater.* **1997**, *45*, 2013–2025. [[CrossRef](#)]
24. Keshavarz Hedayati, M.; Mahboubi, F.; Nickchi, T. Comparison of conventional and active screen plasma nitriding of hard chromium electroplated steel. *Vacuum* **2009**, *83*, 1123–1128. [[CrossRef](#)]
25. Neumann, G.; Tuijn, C. *Self-Diffusion and Impurity Diffusion in Pure Metals: Handbook of Experimental Data*; Pergamon Materials Series 14; Elsevier: Amsterdam, The Netherlands, 2008.
26. Jasinski, J.J.; Fraczek, T.; Kurpaska, L.; Lubas, M.; Sitarz, M. Investigation of nitrogen transport in active screen plasma nitriding processes—Uphill diffusion effect. *J. Mol. Struct.* **2018**, *1164*, 37–44. [[CrossRef](#)]
27. Campos, I.; Torres, R.; Bautista, O.; Ramirez, G.; Zuniga, L. Evaluation of the diffusion coefficient of nitrogen in Fe₄N_{1-x} nitride layers during microwave post-discharge nitriding. *Appl. Surf. Sci.* **2005**, *249*, 54–59. [[CrossRef](#)]
28. Taherkhani, K.; Soltanieh, M. Composite coatings created by new method of active screen plasma nitriding on aluminium alloy 6061. *J. Alloys Compd.* **2018**, *741*, 1247–1257. [[CrossRef](#)]
29. Tessier, F.; Navrotsky, A.; Niewa, R.; Leineweber, A.; Jacobs, H.; Kikkawa, S.; Takahashi, M.; Kanamaru, F.; di Salvo, F.J. Energetics of binary iron nitride. *Solid State Sci.* **2000**, *2*, 457–462. [[CrossRef](#)]

Publisher’s Note: MDPI stays neutral with regard to jurisdictional claims in published maps and institutional affiliations.



© 2020 by the authors. Licensee MDPI, Basel, Switzerland. This article is an open access article distributed under the terms and conditions of the Creative Commons Attribution (CC BY) license (<http://creativecommons.org/licenses/by/4.0/>).